Załącznik nr 3

Presentation of the scientific achievements

Studies on properties of two-dimensional free carrier gas in an external electric or magnetic field

Aneta Drabińska

Division of Solid State Physics, Institute of Experimental Physics,

Faculty of Physics, University of Warsaw

Table of Contents

1. Personal data

    Name: Aneta Drabińska

    Degrees and diplomas:

    > 2004 – Ph.D. in Physics, University of Warsaw, Solid State Physics, thesis title: *Photoreflectance and electroreflectance in low-dimensional nitride structures*.
    > 2000 – Master of Science, Faculty of Physics, University of Warsaw, Solid State Physics.

    Employment:

    > Since 2005: adiunkt, Faculty of Physics, University of Warsaw

2. Scientific achievement

a) Title

> *Studies on properties of two-dimensional free carrier gas in an external electric or magnetic field.*

b) Publication list of scientific achievement

A1. **Aneta Drabińska**, K. P. Korona, K. Pakuła, J. M. Baranowski, "Electroreflectance and Photoreflectance Spectra of Tricolor III-Nitride Detector Structures", Physica Status Solidi (a) 204, 459 (2007), doi:10.1002/pssa.200673965.

A2. Krzysztof P. Korona, **Aneta Drabinska**, Piotr Caban, and Wlodzimierz Strupinski, "Tunable GaN/AlGaN Ultraviolet Detectors with Built-in Electric Field", Journal of Applied Physics 105, 083712 (2009), doi:10.1063/1.3110106.

A3. Krzysztof P. Korona , **Aneta Drabinska**, J. Borysiuk, P. Caban, "Nitride-Based Photodetectors Containing Quantum Wells in Tunable Electric Fields", Journal of Optoelectronics and Advanced Materials 11, 1108 (2009).

A4. **Aneta Drabinska**, Jacek M. Baranowski, Krzysztof Pakula, Piotr Caban, and Wlodzimierz Strupinski, "Electroreflectance Spectroscopy on III-N Quantum Wells", Physica Status Solidi (a) 206, 816 (2009), doi:10.1002/pssa.200881411.

A5. **Aneta Drabińska**, Agnieszka Wołoś, Maria Kamińska, Wlodek Strupinski, and J. M. Baranowski, "Contactless Microwave Studies of Weak Localization in Epitaxial Graphene", Physical Review B 86, 045421 (2012), doi:10.1103/PhysRevB.86.045421.

A6. **Aneta Drabińska**, Maria Kamińska, Agnieszka Wołoś, Włodek Strupinski, Andrzej Wysmołek, Witold Bardyszewski, Rafał Bożek, and J. M. Baranowski, "Enhancement of Elastic and Inelastic Scattering Lengths in Quasi-Free-Standing Graphene Measured with Contactless Microwave Spectroscopy", Physical Review B 88, 165413 (2013), doi:10.1103/PhysRevB.88.165413.

A7. Agnieszka Wolos and **Aneta Drabinska**, "Application of Microwave Spectroscopy to Studies of Electron Transport Properties", Journal of Crystal Growth 401, 314 (2014), doi:10.1016/j.jcrysgro.2013.11.040.

A8. **Aneta Drabińska**, Piotr Kaźmierczak, Rafał Bożek, Ewelina Karpierz, Agnieszka Wołoś, Andrzej Wysmołek, Maria Kamińska, Iwona Pasternak, Aleksandra Krajewska, and Włodek Strupiński, "Electron scattering in graphene with adsorbed NaCl nanoparticles", Journal of Applied Physics 117, 014308 (2015), doi:10.1063/1.4905418.

c) Objectives, results and possible applications of the results presented in publications cited above

Introduction

Due to new phenomena discovered in the field of physics of low-dimensional structures and their potential applications, structures with spontaneous two-dimensional carrier (electron or hole) gas formation are intensively studied nowadays. This includes III-N heterostructures (GaN, AlN, InN and their alloys) in wurtzite structure or graphene. In the case of III-N heterostructures in wurtzite structure, polarization charges located on interfaces due to spontaneous and piezoelectric polarization cause spontaneous formation of two-dimensional electron and hole gas with high concentration and high mobility. In the case of graphene, due to its two-dimensional structure, depositing it on arbitrary substrate creates two-dimensional gas of free carriers; their type and concentration depends strongly on the substrate.

In my work, I studied the properties of spontaneously formed two-dimensional electron and hole gas in external electric or magnetic field using the methods of electric field modulation (photoreflectance and electroreflectance) or magnetic field modulation (microwave spectroscopy). The modulation spectroscopy is based on the concept that an optical spectrum consisting of several broad lines can be reduced to a series of derivative-like lines. The fact that any kind of noise incompatible with the modulation frequency cannot be observed in the spectrum is an additional advantage of these techniques..

Photoreflectance and electroreflectance are the examples of electromodulation reflectance techniques, in which the relative changes of reflectivity coefficient are measured during the modulation of electric field present in the structure. In the case of photoreflectance, the electric field is modulated by a periodic illumination of the investigated structure with laser of energy higher than the energy gap of the investigated semiconductor. Electrons and holes are separated spatially by the electric field present in the structure leading to its reduction. In the case of electroreflectance, electric field modulation is performed by applying the modulation voltage between the semi-transparent Schottky contact evaporated on the structure surface and the conductive substrate.
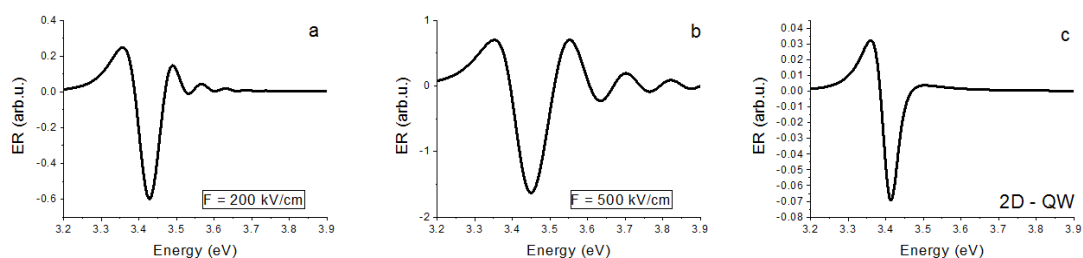

Figure 1. Simulations of photoreflectance/electroreflectance spectrum for layers (for electric field value equal to 200 kV/cm (a) and 500 kV/cm (b)) and quantum wells (c).

The changes of electric field in the investigated structures result in dielectric function perturbation. This leads to the observation of Franz-Keldysh oscillations in the spectrum with period depending on electric field value (figure 1 a and b) [1], [2]. For two-dimensional states, like for example quantum wells, the signal is proportional to the first derivative of reflectivity coefficient on energy of incident light (figure 1 c) [3].

Microwave spectroscopy measurements of two-dimensional electron or hole gas are performed in Electron Paramagnetic Resonance (EPR) spectrometer. Due to the modulation of magnetic field in the resonance cavity, the measured quantity is a derivative of the cavity quality factor on magnetic field. During the classical EPR measurement, the cavity quality factor is changed due to energy absorption for electron spin transitions and the change of magnetization of a sample. However, these are not the only possible reasons for the cavity quality factor changes. They can be induced also by a variation of the sample conductivity. In this case, the recorded signal is proportional to the derivative of the sample conductivity on magnetic field ($d\sigma/dB$). Therefore, for two-dimensional structures, the contactless measurement of magnetoconductance derivative is possible [4], [5].

Studies of tunable UV detectors based on nitride heterostructures

Studies of tunable UV detectors based on nitride heterostructures were the continuation of research performed during my Ph.D. studies. In my Ph.D. thesis, I investigated the properties of two-dimensional electron gas formed spontaneously on AlGaN/GaN interface.

The first conception of the Schottky barrier photodetector based on magnesium-doped p-type GaN films was presented in 1993 by M. Khan [6]. In his work, he presented the photodetector spectral responsivity, which increased by two orders of magnitude after illumination with UV light of energy higher than GaN energy gap. The operation of the detector was based on the deposition of semitransparent Ti/Au Schottky barrier contact, which built the electric field in the surface layer. After illumination of such a structure with light of energy higher than the energy gap of the material, electrons and holes were spatially separated and the voltage between the surface and the conductive substrate was induced.

Figure 2. Operating "solar blind" UV photodetector containing an AlGaN layer. The detector illuminated with day light generates 0.2 mV voltage, whereas after illumination using a mercury lamp, the generated voltage is over 300 mV and can be measured with a universal multimeter.

In my work, I was taking part in a research on extension of this concept by construction of photodetector based on $Al_xGa_{1-x}N$ layer. With a proper selection of the layer composition (x), the photodetector can be sensitive to the corresponding value of incident light energy. In particular, the layer composition can be chosen in such a way that the detector is not sensitive to the visible light but only to the UV light (*visible blind photodetector*). The composition can be also chosen in such a way that the detector is

not sensitive to solar light but only to high energy UV light (*solar blind photodetector*). An example of an operating solar blind UV photodetector, constructed at the Faculty of Physics, University of Warsaw, is presented in Figure 2. The detector is insensitive to the day light, but after illumination with a mercury lamp, it generates voltages measurable with a universal multimeter.

The next step was the construction of a UV photodetector with sensitivity tunable by voltage. The conception of such a photodetector was to grow N successive undoped $Al_{x0}Ga_{1-x0}N$, …, $Al_{x(N-1)}Ga_{1-x(N-1)}N$, $Al_{xN}Ga_{1-xN}N$ layers, with $0 = x0 < … < xN \leq 1$, on a conducting n-type GaN layer. Such a construction firstly increases the energy gap in subsequant layers and secondly, due to spontanous polarization, the positive polarization charge is present on each interface. The positive polarization charges attract free electrons, which spontanously form two-dimensional electron gas on each interface. Futhermore, in an unpolarized state, the electric field in each layer is screened (Figure 3 a) and the detector is inactive. Although illumination with light of energy higher than the GaN energy gap creates electron-hole pairs, they recombine fast.
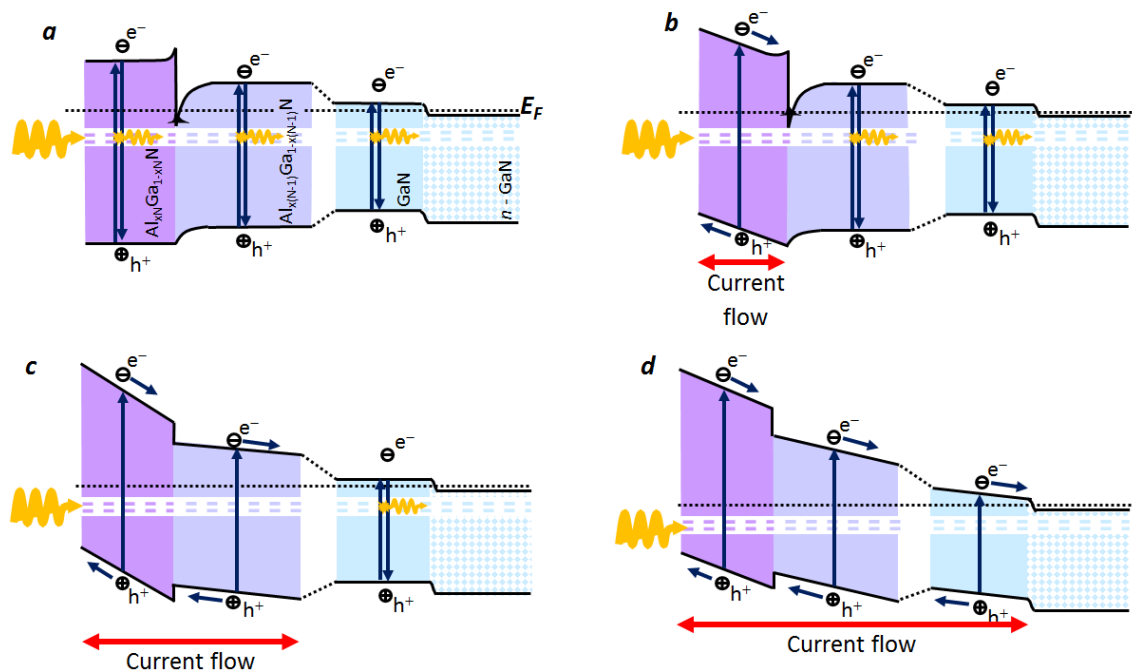

Figure 3. The scheme of tunable UV photodetector band structure.

The situation changes after evaporating a semitransparent metallic contact which makes Schottky diode. In this case, in the first layer with the highest energy gap (E_N), electric field is built in. Electron-hole pairs created after illumination of the photodetector with light of energy higher than this energy gap are separated by the electric field and current flow can be observed (Figure 3 b). Applying a reverse bias between the Schottky diode and the conductive substrate builds higher electric field in the structure. At some point, the electric field is large enough to deplete electon gas from the interface between N and $N-1$ layers and to build electric field into the $N-1$ layer. In this case, the current flow is induced by ilumination of the photodetector with light of energy higher than $E_{N-1} < E_N$ (Figure 3 c). By applying higher voltage, the electron gas can be depleted from subsequent interfaces and the electric field can be build into

succesive layers. With increasing reverse voltage, the energy of activating light decreases up to the value corresponding to the GaN energy gap (figure 3 d).

The operation of such a detector, although conceptually simple, is non-trivial due to existing spontaneous and piezoelectric polarization. Theoretical polarization calculations predicted very high electric field values in nitride structures [7]–[9]. The experiment, however, suggested rather screening of those electric fields by free carriers present in the structures [10]–[12]. Additionally, the presence of defects caused the strain relaxation in the structure and the prediction of piezoelectric polarization value was not accurate. Therefore, the photoreflectance and electroreflectance techniques, in which the lineshapes depend on the value of electric field, were very promising in research on such detector structures.

Detectors consisting two and three active $Al_xGa_{1-x}N$ layers were chosen as basic detector structures for these studies. In the first layer, Al composition was $x = 0$ (GaN layer) and the aluminium content was gradually increasing. [A1] and [13] present the photoreflectance, electroreflectance, theoretical modeling, photocurrent and direct current investigations for a detector containing three active layers: GaN, $Al_{0.1}Ga_{0.9}N$ and $Al_{0.2}Ga_{0.8}N$. In [A2], the theoretical modeling, electroreflectance, photocurrent and current-voltage characteristics were presented for the detector with two active layers: GaN and $Al_{0.23}Ga_{0.77}N$ and compared to a detector containing three active layers: GaN, $Al_{0.15}Ga_{0.85}N$ and $Al_{0.27}Ga_{0.73}N$.

Preliminary characterization and estimation of electric field values were performed on structures without the Schottky contact using photoreflectance. An example of a photoreflectance spectrum is presented in figure 3 in [A1]. The lineshapes for all layers are characteristics for low electric field regime. This proves the screening of electric field by free electrons attracted to the interfaces. Upon fitting a theoretical model, the energy gaps of each layer and also the energies of light, which detector is sensitive to, could be determined. Additionally, lines originating from transitions within the two-dimensional electron gas on each interface were observed. Hence it was possible to determine the energy states in triangular quantum wells (QWs) spontaneously formed on the interfaces.

Electroreflectance spectrum of the investigated photodetector had different character depending on the voltage applied to the Schottky diode (i.e. Fig. 5 in [A1]). For a detector with three active layers, for forward bias and low reverse bias, two features are observed in spectrum. First of them are Franz-Keldysh oscillations (FKOs) from the top layer (with the highest energy gap) and second is a low amplitude line from the second layer, characteristic for low electric field regime. Therefore, for this bias range, two-dimensional electron gas is present on the first interface and electric field is built only in the first active layer. For higher reverse bias, the line from the second layer changes its character and FKOs are observed. At the same time, the weak line characteristic for low electric field regime is observed for energies corresponding to energy gap of the last active layer – the GaN layer. This shows the depletion of electron gas from the first interface; the electric field is built to the second active layer but the two-dimensional electron gas located on the second interface screens the electric field in GaN layer. Asymptotic expansion of Airy function shows that FKOs are periodic as a function $\left(E - E_g\right)^{3/2}$, where E_g is material energy gap with period depending linearly on the electric field value. Due to the increasing electric field value, the observed FKOs period increased with reverse bias.

In [A1], using Fourier transform, the electric field dependence on the applied voltage was calculated and voltage for which the electron gas is depleted from the specified interface was determined. It was shown that the electric field is uniform in each layer and depends linearly on the applied voltage and hence the thickness of the individual layers could be determined. The difference between the electric fields values in the individual layers provided the surface density of polarization charge located on the interface and the difference of total polarization between the layers.

When the distribution of the electric field and the polarization charge were known, self-consistent calculations could be performed and furthermore the band structure, electrons and holes concentration, and the current flowing in the detector upon application of different bias and illumination could be determined. Fundamentals of theoretical modeling were thoroughly described in [A2]. The results of the numerical modeling show that, in the case of unilluminated and unpolarized structure, electrons are localized in the doped GaN layer and on interfaces between the individual layers. Electrons localized on the interfaces screen the electric field in the layers other than the one nearest to the surface. Upon application of a few volts of reverse voltage to the Schottky diode, the concentration varies by more than one order of magnitude, effectively depleting electrons from the interface. Calculations for the illuminated sample show that the electron current depends slightly on the applied voltage, whereas the applied reverse voltage significantly affects the hole transport (fig. 2 in [A2]). For small reverse bias, holes encounter a barrier on individual interfaces, and they recombine with electrons. Due to the fact that the concentration of photo-induced holes is several orders of magnitude smaller than the concentration of the polarization-induced electrons located on the interfaces, this recombination has no significant effect on the electron transport in the structure. Only for large reverse bias, holes can freely flow to the sample surface.

Research on spectral dependence of the illuminated detector response was the next step. The photocurrent spectrum showed a very clear dependence on the applied voltage (e.g. Fig. 4 in [A2]). In the case of an unpolarized detector, photocurrent is generated only after the detector is illuminated with light of energies higher than the band gap of the surface layer. Applying reverse voltage moves the detector sensitivity progressively to the lower energies. "Switching on" successive detector layers increases the detector sensitivity to light corresponding to the bandgap of these layers by more than one order of magnitude. The detector response for not very high intensities of light (up to approx. 1 mW/cm^2) is linear. For higher power densities, nonlinear detector response was observed, most likely due to screening of the electric field by a high concentration of photocarriers. The direct-current (DC) studies have shown that in the case of a small area of the Schottky contact (less than 1 mm^2), the influence of different light energy on the measured current is clearly observed (Fig. 5 in [A2]). In the case of a large area of Schottky contact (above 10 mm^2), due to a large leakage current, the discussed effect was observed only for a small reverse voltage (Fig. 8 in [A1]). For higher reverse voltage, leakage current was higher than the current generated by light and it was impossible to observe the desired effects. Most likely, it was related to a larger amount of conductive dislocations covered by the Schottky contact.

The studies on detector structures containing quantum wells in the cavity were the next step considering nitride detector structures. The results were described in [A3] and [14]. The investigated structures were as follows: In$_{0.1}$Ga$_{0.9}$N QW well in Al$_{0.05}$Ga$_{0.95}$N

cavity surrounded by $Al_{0.15}Ga_{0.85}N$ barrier and two GaN QWs in $Al_{0.1}Ga_{0.9}N$ cavity surrounded by $Al_{0.2}Ga_{0.8}N$ barrier. The detector structure was designed to separate photo-induced carriers by the electric field and change the cavity potential. Studies of such structures has shown that not only the intensity of the photocurrent but also its direction depends on the applied voltage. Charge accumulation in the structure allowed fast recombination of electrons and holes and the change of the electric field inside the active region. This shows the possibility of the detector to be tuned by light. In the case of illumination of such a detector with two light sources of different energies, its response depends on both sources. In the case of the structure with a single quantum well, the illumination with two different light sources resulted in signal gain over a wide energy range. The response of the detector was larger, as compared to that for each of the light sources separately. This kind of detector can be treated as the optical equivalent of the AND electrical conjunction gate. In the case of a double quantum well, the detector structure response to light from only one of the sources is positive while in the case of double source illumination, detector signal attenuation was observed. This structure is hence an optical equivalent of XOR exclusive gate.

Quantum-confined Stark effect in nitride quantum wells studies

In the case of nitride quantum wells, due to the existence of spontaneous and piezoelectric polarization, polarization charges of opposite sign are built-in on both sides of the quantum wells. Therefore, in the quantum well, a built-in electric field adds linear potential. When an external electric field is applied, the electron states shift to lower energies, while the hole states shift to higher energies. This reduces the permitted light absorption or emission energy. Additionally, the electric field shifts electrons and holes to opposite sides of the well, decreasing the overlap integral, which in turn reduces the recombination efficiency. In my work, I focused on electroreflectance and luminescence studies of quantum wells, for which the built-in electric field could be modified by applying an external voltage to the semitransparent Schottky contact. The results were described in [A3], [A4], and [14]–[16].

In the case of a structure containing a single quantum well, with no external voltage applied, lines originating from transition within the quantum well and Franz-Keldysh oscillations from the barriers are observed in the electroreflectance spectrum (e.g. Fig. 1 in [A4]). A detailed analysis of FKOs shows that two overlapping oscillations with very close frequencies are present in the spectrum. This shows two different values of electric field in barriers on both sides of the quantum well. The difference of these electric field values (ΔF) is related to the electric charge of the concentration $n = \Delta F \varepsilon \varepsilon_0 / e$ present in the quantum well. The charge induced by the different polarization of the quantum well and barrier is located on both QW/barrier interfaces and has the same value but the opposite sign on each interface. Therefore, it cannot cause different electric field values in barriers. Thus, the difference in electric field values can only origin from electrons and holes occupying QW quantum states (eg. fig. 2 a in [A4]).

The electric field induced in the quantum well by the spontaneous and piezoelectric polarization has an opposite direction with respect to the electric field in barriers and electric field built by the reverse voltage applied to the Schottky diode. Therefore, along with the applied reverse voltage, the electric field in the barriers increases. This can be observed as an increasing period of the Franz-Keldysh oscillations from barriers with increasing reverse bias. The obtained electric field value in the barriers increases linearly with the applied reverse voltage. For high reverse voltage, due

to large built-in electric field, the barrier has a triangular shape. This, by increasing the probability of carriers tunneling from the quantum well to the barrier, reduces the occupation of quantum states in QW (e.g. Fig. 2 c in [A4]) and one frequency of FKOs is observed.

Application of a reverse voltage in the quantum wells first decreases the electric field in the quantum well. For a certain voltage, the external electric field screens the polarization-induced electric field. For this voltage, the effective electric field in the quantum well is zero. When the higher reverse voltage is applied, the electric field is again built into the quantum well but with a direction opposite to the spontaneous field. In [A4] and [16], fit of the theoretical model allowed determination of the energy, amplitude and broadening parameter of transition lines as a function of the applied voltage. By analyzing Franz-Keldysh oscillation from barriers, it was possible to relate the electric field to the applied voltage. Furthermore, it was possible to determine the energy, amplitude and broadening parameter of transition lines in quantum well as a function of the electric field in the quantum well. It was shown that with the electric field in the quantum well completely screened, the line the from quantum well was not observed in the spectrum. With the increasing electric field, the line amplitude also increases but its width decreases. The signal phase is changed to the opposite upon change of the electric field direction. The Schrödinger equation with a linear potential $V = -eFz$ has to be solved to calculate the electron and hole quantum state energies. In the case of an infinite square quantum well, the solution is a sum of Airy functions, and for small values of electric fields and small width of the wells (i.e. for which the potential built by an electric field along the quantum well width is much smaller than the energy of carriers in the quantum well), it can be approximated by quadratic dependence of the electron and hole energies on the electric field. In [A3], [A4], it was shown that this approximation describes well the Stark shifts observed in electroreflectance and luminescence measurements. Additionally, in [16], it was shown that this simple quadratic dependence also applies to quantum wells, for which the assumption of small electric field and small quantum well width is not fulfilled. However, in this case, the obtained coefficients are not defined by equation (2) in [A3].

Microwave studies on graphene conductivity

Interesting physical properties and potential applications of graphene made this material one of the most intensively studied nowadays. Its unique physical properties resulting from its crystal structure were already described in the forties of the twentieth century [17]. However, just experiments showing the possibility to obtain a single, two-dimensional graphene layer and measurements of the predicted by theory properties [18], [19] resulted in the enormous and growing interest in research on graphene. Studies reflecting the quantum and chiral nature of carriers in graphene are the most interesting. In my work, I focused on contactless magnetotransport studies. In particular, I studied electron quantum interference effects in graphene, resulting in weak localization and weak antilocalization effects. The results were published in [A5]–[A8] and [20]–[22].

The effects of a weak localization or antilocalization are often observed in structures with a two-dimensional electron gas. Their observation is possible due to the imperfections of the system, in which the scattering centers are present. The basic concept of this effect is the interference of two wave functions of electrons scattered along a closed loop in opposite directions [23]. Constructive interference is taking place

if the phases of the wave functions at the point of interception are identical. This increases the probability of an electron to be backscattered and results in an increase in resistance and a decrease in conductivity of the two-dimensional gas. This effect is called a weak localization. If the phases of the electron wave functions are opposite, destructive interference takes place. In this case, the probability of forward scattering increases, which in turn results in a decrease in resistance and an increase in the conductivity of the electron gas. This effect is called weak antilocalization. The effect of the weak localization or antilocalization is observed experimentally only in case when electron travelling on the closed loop maintains its phase – i.e. non-elastic scattering responsible for electron decoherence is small. Since more carriers can take part in the effect when coherence length increases, this phenomenon is observed at low temperatures, for which the coherence length is greater than scattering lengths. In the case of graphene, the theory describing weak localization/antilocalization effect must consider the chiral nature of carriers associated with an additional quantum number – pseudospin. In graphene, due to electron Berry's phase of π – an additional phase the electron receives after completing a closed loop, the weak antilocalization effect is expected. However, the first experiments did not confirm these predictions and the weak localization was observed [24]. Finally, a theory describing the effects of weak localization and antilocalization, taking into account the additional elastic scattering was presented [25]. Since an elementary cell of the lattice has a basis of two atoms, the wave function has an effective 2-spinor structure. This leads to the Dirac cones in two non-equivalent points in Brillouin zone (K and K'). Elastic scattering on the long range potential or p$\rightarrow$−p symmetry breaking destroys the weak antilocalization effect. In addition, elastic scattering between the two Dirac cones changes electron pseudospin and introduces the typically observed weak localization. Thus the observation of either weak localization or antilocalization in a specific graphene sample depends on the type of the dominant scattering process.

Studies of weak localization/antilocalization effects are carried out as a function of magnetic field. Magnetic field destroys interference effects by adding its own phase to the electron wave function. This can be observed as a negative magnetoresistance (positive magnetoconductivity) in the case of weak localization and positive magnetoresistance (negative magnetoconductivity) in the case of weak antilocalization. In my work, together with dr. Agnieszka Wołoś, I set-up EPR measurement technique in Faculty of Physics at University of Warsaw. The system is equipped not only in standard microwave X band, but also in Q-band microwaves (about 35 GHz) and pulse EPR technique. It was also extended to allow measurements of electrically detected magnetic resonance (EDMR). Next I was leading research concerning graphene and non-standard contactless measurements of $d\sigma/dB$ using EPR spectrometer. This method was proposed for the measurement of weak localization effect for the first time in [A5]. A typical spectrum measured at 2 K with integrated signal corresponding to the conductivity is presented in Fig. 1 in [A5]. A characteristic signal from weak localization is observed against a classical Drude conductivity background signal. By fitting the theoretical model presented in [25], the coherence length and elastic intervalley and long-range scattering lengths could be determined. Since a non-standard technique was used, it was very important to investigate the influence of the technique itself on the measurement results. In particular, in EPR spectrometer, three different magnetic fields are present (fig. 4): magnetic field as a function of which the signal is measured (B_0),

modulating magnetic field (B_1) perpendicular to B_0, with a frequency of approx. 100 kHz and microwave magnetic field (B_f) of a frequency of approx. 9.5 GHz.
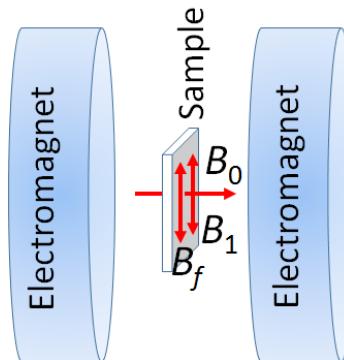

Figure 4. Magnetic fields in EPR spectrometer.

In order to optimize the proposed technique for weak localization/antilocalization measurements, the signal was measured as a function of modulation amplitude and microwave power (Fig. 2 in [A5]). It was shown that the amplitude of the measured signal depends linearly on the modulation amplitude for the entire range available in spectrometer (up to 1 mT). The amplitude of the signal depends also linearly on the square root of the microwave power for power less than approx. 4 mW; for higher microwave power, the saturation and broadening of the signal was observed, which is most likely associated with heating of the sample.

Since a weak localization signal is derived from two-dimensional electron gas, it depends on the magnetic field component perpendicular to the plane of the two-dimensional gas. Therefore, the angular dependence of the signal amplitude and width was examined (Fig. 4 in [A5]). It was shown that the width of the signal is inversely proportional to the cosine of the angle between the normal to the surface of the two-dimensional gas and the magnetic field. For a wide range of angles around zero, it changes very slightly. The amplitude of the signal showed the cosine square dependence of that angle. This demonstrates an additional reduction in signal amplitude, as compared to the one predicted based on the magnetic field normal component.

Thus, although the amplitude of the signal depends on the measurement parameters, the obtained values of coherence and elastic scattering lengths are reliable, regardless of the measurement conditions.

In my work, I focused on measurements of CVD graphene samples on silicon carbide (SiC) substrate grown at the Institute of Electronic Materials Technology (Warsaw, Poland). The crystal structure of SiC, similar to GaN, is a hexagonal structure, i.e. it is associated with inversion symmetry breaking. Consequently, two polarities can be distinguished in this structure: (0001) – silicon face of SiC and (000-1) – carbon face of SiC. Dynamics and conditions of the graphene growth on various SiC polarities are significantly different. In particular, in the case of graphene grown on the carbon face of SiC, growth rate is large, therefore, there are always more than one graphene layer present. However, due to the azimuthal disorientation of the individual layers, they can be considered as several independent graphene layers rather than graphite [26], [27] (Figure 5a). The growth on silicon face of SiC is much slower, therefore, a single graphene layer can be easily grown. This is very important since graphene layers on silicon face are Bernal stacked, which results in interactions between the individual layers.

Additionally, the first layer of carbon atoms is strongly coupled to the substrate via sp^3 bonds. It is an electrically inactive so-called buffer layer [28], [29] (Fig. 5b). The next layer of carbon atoms have already sp^2 hybridization and properties of a graphene layer. sp^3 bonds in the buffer layer are responsible for strong interaction of graphene with the substrate. Therefore, hydrogen intercalation has been recently proposed as a method of delamination of the buffer layer from the substrate [30]. The hydrogen atoms diffuse in between the buffer layer and the substrate and saturate the silicon surface states of SiC substrate. Consequently, carbon atoms in the buffer layer after the hydrogen intercalation have mostly sp^2 hybridization, and this layer has the properties of a graphene layer (Fig. 5c).
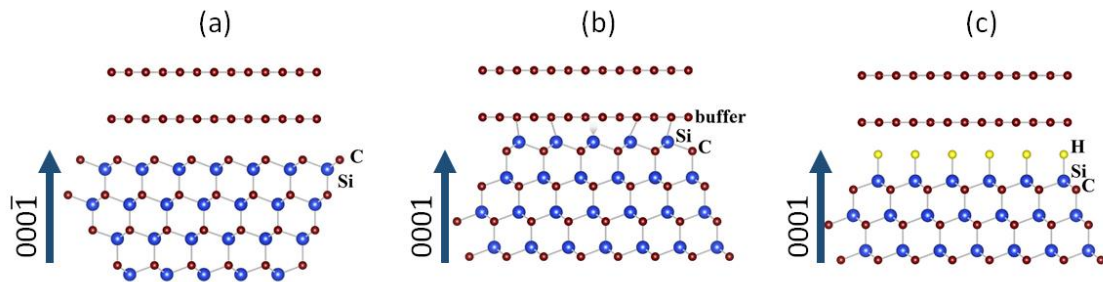

Figure 5. Crystal structure of graphene grown on C-face SiC (a), Si-face SiC (b) and Si-face SiC with additional hydrogen intercalation. Figures prepared using VESTA program [31].

In [A6], weak localization/antilocalization signals for graphene layers obtained on silicon and carbon face of SiC with and without the hydrogen intercalation were compared. For small magnetic fields (less than 50 mT), for all graphene sample types, weak localization manifested by positive magnetoconductivity was observed. For higher magnetic fields, for graphene grown on silicon face of SiC, the signal was close to zero. For graphene grown on carbon face of SiC, the signal changed its sign and for higher magnetic fields weak antilocalization contribution to the signal and negative magnetoconductivity was observed (Fig. 1 in [A6]). In the case of graphene not intercalated with hydrogen, width of weak localization signal was comparable for both samples (graphene on carbon and silicon face of SiC) and it was about one order of magnitude wider than in the case of hydrogen intercalated graphene. At the same time, the amplitude of the signal for not intercalated samples was about one order of magnitude smaller than the amplitude for the intercalated samples. Since the width and the inverse amplitude of the weak localization line is proportional to the decoherence field (Fig. 3b [A5]), much longer coherence lengths were observed after hydrogen intercalation. By fitting the theoretical model, it was possible to determine the coherence and characteristic elastic scattering lengths. For all three graphene types, the dominant scattering is elastic long-range scattering. Long range scattering lengths did not exceeded 50 nm in any case. However, its slight increase for graphene grown on carbon face of SiC and hydrogen intercalated graphene grown on silicon face of SiC was observed (lengths approx. 30-40 nm), as compared to not intercalated graphene on silicon face of SiC (lengths approx. 10 nm). The elongation of elastic intervalley scattering lengths from approx. 100 nm, typical for not intercalated graphene grown on silicon face of SiC [32], [33], to over one micrometer for graphene weakly coupled to the substrate (both: hydrogen intercalated graphene on silicon face of SiC and graphene grown on carbon face of SiC) was a very interesting observation. This demonstrates not only a dramatic reduction of this type of scattering, but also an important role of the

interactions with the substrate in this scattering. The observed elongation of intervalley scattering length suggests the change from substrate to grain boundary dominated scattering mechanism. While the elastic scattering depends on the crystal defects, and therefore is temperature independent, the temperature dependence of the coherence length gives information about inelastic scattering mechanisms. For all three types of samples, temperature dependence of the coherence length indicates the electron-electron scattering: for hydrogen intercalated samples in ballistic regime and for other samples in diffusion regime (Fig. 2 in [A6]). In the case of not intercalated graphene, temperature independent offset in linear temperature dependence of decoherence field was observed, showing additional inelastic scattering process. This resulted in a significantly reduction of the coherence length to approx. 200-300 nm at 2 K compared to approx. 1 μm for hydrogen intercalated graphene. As a possible mechanism, spin relaxation during scattering on defects carrying localized magnetic moment was proposed [34], [35].

The occurrence of either weak localization or antilocalization depends on the relative strength of inelastic and elastic scatterings. In [A6], the conditions of the observation of each effect separately or both effects together (for small magnetic fields the effect of a weak localization and for higher magnetic field weak antilocalization) (Fig. 3 in [A6]) were discussed. As it can be seen in the phase diagram of weak antilocalization to weak localization transition, weak coupling of graphene to the SiC substrate leads to a reduction of the ratio of coherence and elastic intervalley scattering lengths by about one order of magnitude. On the other hand, the significant increase of coherence length only for hydrogen intercalated graphene and at the same time a slight increase of long range elastic scattering for graphene grown on the carbon face of SiC and hydrogen intercalated graphene on silicon face of SiC make the observation of a weak antilocalization simultaneously with the weak localization possible only for samples grown on the carbon face of SiC.

The impact of the external environment on weak localization signal in graphene was yet another aspect of my research. In [A8], the results of weak localization measurements after immersing graphene in 0.1 M NaCl solution were presented. Surface functionalization of graphene with NaCl nanocrystals was confirmed by atomic force microscopy and EPR spectroscopy. Weak localization studies showed that deposition of nanocrystals NaCl on the graphene surface did not affect neither the long range nor the intervalley scattering lengths. After NaCl immersion of graphene there was, however, a significant reduction in the electron coherence length. The temperature dependence of the coherence length showed electron-electron scattering as the main electron decoherence mechanism and the change from ballistic to diffusive regime of electron transport. The main reason of electron coherence length reduction after NaCl graphene treatment was found, however, to be additional temperature independent elastic scattering. It was related to the presence of magnetic ions on the graphene surface responsible for electron spin relaxation. This confirmed the hypothesis proposed in [A5]–[A7]. Additional information about the nature of the defects created after graphene functionalization with NaCl nanocrystals were provided by Raman spectroscopy studies. Statistical analysis of intensities of Raman bands showed that additional scattering is caused by both: the decoration of existing defects (vacancies and grain boundaries) with NaCl particles and the formation of new defects in the graphene crystal lattice structure by decoration of its surface with NaCl molecules. Additionally,

analysis of the Raman bands energy showed that the functionalization of graphene molecules NaCl did not change the carrier concentration, but reduced stress in the graphene layer.

In [A5] and [A7], classical Drude conductivity observed as a background of strong weak localization signal was also discussed. For low mobility graphene, for the entire range of magnetic fields available in EPR spectrometer (up to 1.7 T), it was observed as a linear background (fig. 1a [A5]). Due to the signal amplitude dependence on the measurement parameters (modulation amplitude and microwave power), it was not possible to determine electron mobility in this case. However, for samples with higher electron mobility, Drude signal is no longer linear (Fig. 5 in [A7]). Fit of $d\sigma/dB$ presented in [A7] allowed determination of the mobility of electrons equal to 4,000 cm^2/(Vs), which is consistent with the values obtained in classical magnetotransport measurements.

Summary

The presented research concerned two-dimensional carrier gas studies formed in particular on interfaces or in quantum wells (nitride structures) and in graphene.

In the case of nitride structures, the properties of electron gas in an external electric field were studied using electroreflectance and photoreflectance methods. Electron concentration as a function of the external electric field of the two-dimensional electron gas located in the triangular potential wells formed spontaneously on interfaces, as well as in intentionally grown square quantum wells, were observed.

Application of two-dimensional electron gas formed spontaneously in nitride heterostructures in a tunable UV detector structures was presented. A thorough study and theoretical modeling of carrier concentration, electric fields and current in these detectors was performed.

Quantum-confined Stark effect in the square quantum wells was investigated. Line energy, intensity and broadening parameter related to the carriers lifetime in the well, were discussed as a function of the electric field in the well. The experimental results were compared with theoretical predictions, and discussed considering the quantum well width.

In the case of electrons in graphene, the research focused on contactless magnetoconductivity measurements performed using microwave spectroscopy in EPR spectrometer.

The studies covered mostly effects of weak localization and weak antilocalization of free carriers in graphene. Various elastic scattering mechanisms in the samples strongly and weakly coupled with a substrate were discussed. It was shown that one of the mechanisms responsible for inelastic scattering and decoherence of free carriers in epitaxial graphene is electron-electron scattering. In addition, a second inelastic scattering mechanism causing significant reduction in the coherence length to hundreds of nanometers was found. As a possible mechanism, scattering on defects carrying localized magnetic moment was proposed. It was proved that this scattering vanishes after hydrogen intercalation and electron-electron transport turns into the ballistic regime in this case. The conditions of weak localization and weak antilocalization observation as a function of the ratios of inelastic and elastic scattering lengths were also discussed.

For high mobility samples, classic Drude magnetoconductivity observed in contactless EPR spectrometer provided the possibility to determine the mobility of electrons in graphene.

3. Other scientific achievements.
    Before Ph.D. degree
    I started my Ph.D. studies in 2000 with the construction of electroreflectance and photoreflectance set-up designed for nitride structures measurements. Preliminary luminescence results from nitride quantum wells did not confirm the theoretical predictions of the built-in electric fields based on spontaneous and piezoelectric polarizations. Therefore, it was very important to extend the nitride studies with the use of techniques capable of measuring the electric field values in these materials directly. The constructed system was tested using gallium arsenide structures with two-dimensional doping outside the quantum well [36]. Next, I performed research on nitride structures. Initially, these were focused on the determination of concentration of two-dimensional electron gas intentionally doped [37] or induced spontaneously in AlGaN/GaN heterostructures [12], [38]. This demonstrated the adequacy of electromodulation techniques for measurement of such structures. In particular, photoreflectance measurements showed screening of electric field by free carriers located on theses interfaces. Hence, I could also determine the energy transitions in spontaneously formed triangular potential wells at AlGaN/GaN interface.

    In the case of Schottky barrier electroreflectance, analysis of electric fields in the individual layers allowed the concentration of free electrons localized on interfaces to be determined. The possibility of depleting electrons from interfaces by applying a voltage was shown. This in turn led to determination of the surface concentration of charges induced by spontaneous and piezoelectric polarization and comparison of the obtained values with the theoretical calculations. Additionally using X-ray diffraction, it was possible to determine the actual lattice parameters and also the piezoelectric polarization value. Consequently, the value of the spontaneous polarization difference between the layers in the investigated heterostructures was found.

    After Ph.D. degree
    After Ph.D. degree, one of the scientific topics I was working on were studies on the optical absorption by graphene. A single isolated graphene layer absorbs 2.3% of white light. In the case of graphene grown on SiC substrate, the main contribution to the absorption is the substrate itself with its macroscopic thickness. Therefore, in the case of graphene on a SiC substrate, the measured transmission must be normalized to the transmission of the substrate itself. Transmission as a function of incident light wavelength for epitaxial graphene grown on SiC substrate for samples with different number of graphene layers was presented in [39]. It was shown that graphene transmission depends only slightly on the wavelength of the incident light in the range between 600 nm and 1,150 nm. It was also shown that even for a very large amount of graphene layers (tens of layers), absorption depends linearly on the layer number. This technique was used to determine the number of graphene layers in several papers. It was used as the primary measurement technique in investigations of graphene layer growth kinetics [40], [41]. The dependences of growth rate on the reactor conditions (gas pressure), growth time, the polarity of the SiC substrate, microscopic quality, etc. were discussed in these papers. It was shown that the growth kinetics is limited by the

evaporation rate and diffusion of the silicon atoms from the substrate. In [42], the correlation of graphene layer number obtained from the transmission with an intensity of 2D Raman band was examined. In [43], it was used as one of the characterization techniques of graphene weakly and strongly coupled to the substrate. The correlations between the different methods used to determine the number of graphene layers (optical absorption, Raman spectroscopy and X-ray diffraction) were presented in [44].

Other studies in which I was involved included the spin and magnetoplasma resonance studies in AlGaN/GaN heterostructures described in [45] and [A7]. In these papers, the Rashba effect in bulk GaN and AlGaN/GaN heterostructures was discussed. Magnetoplasma resonance and Shubnikov-de Haas oscillations in heterostructures with different mobility of two-dimensional electron gas and the possibility of determination of electron concentration, mobility or effective mass were presented. Weak localization measurement of a two-dimensional electron gas at the AlGaN/GaN interface allowed electron coherence time, a spin-orbit interaction constant and Rashba parameter of spin-orbit interaction to be determined.

Moreover, I was involved in the microwave studies of three-dimensional topological insulators Bi_2Te_3, Bi_2Se_3 and Bi_2Te_2Se presented in [46], [47] and [A7]. In these papers, cyclotron resonance observed in Bi_2Te_3 was presented and the electron Fermi velocity was determined. Weak antilocalization measurement from two-dimensional surface electrons in Bi_2Te_2Se allowed the coherence length and its temperature dependence to be obtained. Additionally, these papers include the results of Shubnikov-de Hass oscillations in Bi_2Te_3 and spin resonance in Bi_2Se_3 from the bulk electrons. Based on the Shubnikov-de Hass oscillations frequency, the Fermi energy in this material could be determined. Spin resonance measurement allowed the accurate determination of the electron g-factor in Bi_2Te_3 and its magnetic field dependence.

4. References

[1]   M. Cardona, K. Shaklee, and F. Pollak, "Electroreflectance at a Semiconductor-Electrolyte Interface," *Phys. Rev.*, vol. 154, no. 3, pp. 696–720, Feb. 1967.

[2]   D. Aspnes, "Band nonparabolicities, broadening, and internal field distributions: The spectroscopy of Franz-Keldysh oscillations," *Phys. Rev. B*, vol. 10, no. 10, pp. 4228–4238, Nov. 1974.

[3]   B. Shanabrook, O. Glembocki, and W. Beard, "Photoreflectance modulation mechanisms in GaAs-Al_{x}Ga_{1-x}As multiple quantum wells," *Phys. Rev. B*, vol. 35, no. 5, pp. 2540–2543, Feb. 1987.

[4]   H. Linke, P. Omling, P. Ramvall, B. K. Meyer, M. Drechsler, C. Wetzel, R. Rudeloff, and F. Scholz, "Application of microwave detection of the Shubnikov–de Haas effect in two-dimensional systems," *J. Appl. Phys.*, vol. 73, no. 11, p. 7533, 1993.

[5]   H. A. F. Charles P. Jr. Poole, *Handbook of Electron Spin Resonance*. Springer, 2007.

[6]   M. Asif Khan, J. N. Kuznia, D. T. Olson, M. Blasingame, and a. R. Bhattarai, "Schottky barrier photodetector based on Mg-doped p-type GaN films," *Appl. Phys. Lett.*, vol. 63, no. 18, p. 2455, 1993.

[7]   F. Bernardini, V. Fiorentini, and D. Vanderbilt, "Spontaneous polarization and piezoelectric constants of III-V nitrides," *Phys. Rev. B*, vol. 56, no. 16, pp. R10024–R10027, Oct. 1997.

[8]   O. Ambacher, J. Smart, J. R. Shealy, N. G. Weimann, K. Chu, M. Murphy, W. J. Schaff, L. F. Eastman, R. Dimitrov, L. Wittmer, M. Stutzmann, W. Rieger, and J. Hilsenbeck, "Two-

dimensional electron gases induced by spontaneous and piezoelectric polarization charges in N- and Ga-face AlGaN/GaN heterostructures," *J. Appl. Phys.*, vol. 85, no. 6, p. 3222, 1999.

[9]   O. Ambacher, J. Majewski, C. Miskys, A. Link, M. Hermann, M. Eickhoff, M. Stutzmann, F. Bernardini, V. Fiorentini, V. Tilak, B. Schaff, and L. F. Eastman, "Pyroelectric properties of Al(In)GaN/GaN hetero- and quantum well structures," *J. Phys. Condens. Matter*, vol. 14, no. 13, pp. 3399–3434, Apr. 2002.

[10]   T. Takeuchi, C. Wetzel, S. Yamaguchi, H. Sakai, H. Amano, I. Akasaki, Y. Kaneko, S. Nakagawa, Y. Yamaoka, and N. Yamada, "Determination of piezoelectric fields in strained GaInN quantum wells using the quantum-confined Stark effect," *Appl. Phys. Lett.*, vol. 73, no. 12, p. 1691, 1998.

[11]   P. Perlin, C. Kisielowski, V. Iota, B. A. Weinstein, L. Mattos, N. A. Shapiro, J. Kruger, E. R. Weber, and J. Yang, "InGaN/GaN quantum wells studied by high pressure, variable temperature, and excitation power spectroscopy," *Appl. Phys. Lett.*, vol. 73, no. 19, p. 2778, 1998.

[12]   A. Drabińska, "Photo- and Electroreflectance Spectroscopy of Low-Dimensional III-Nitride Structures," *Acta Phys. Pol. A*, vol. 104, no. 2, p. 149, 2003.

[13]   K. P. Korona, A. Drabińska, K. Pakuła, and J. M. Baranowski, "Multiband GaN / AlGaN UV Photodetector," *Acta Phys. Pol. A*, vol. 110, no. 2, pp. 211–217, 2006.

[14]   K. P. Korona, A. Drabińska, K. Surowiecka, L. Wołowiec, J. Borysiuk, P. Caban, and W. Strupinski, "InGaN QW in External Electric Field Controlled by Pumping of 2D-Electron Gas," *Acta Phys. Pol. A*, vol. 114, no. 5, pp. 1179–1186, 2008.

[15]   A. Drabińska, K. Pakuła, J. M. Baranowski, and I. Frymak, "Electroreflectance and photoreflectance studies of AlGaN/GaN heterostructure with a QW placed inside AlGaN layer," *Phys. status solidi*, vol. 202, no. 7, pp. 1308–1312, May 2005.

[16]   A. Drabińska, K. Pakuła, J. M. Baranowski, and A. Wysmołek, "Electroreflectance investigations of quantum confined Stark effect in GaN quantum wells," *J. Phys. Conf. Ser.*, vol. 253, p. 012009, Nov. 2010.

[17]   P. Wallace, "The Band Theory of Graphite," *Phys. Rev.*, vol. 71, no. 9, pp. 622–634, May 1947.

[18]   K. S. Novoselov, A. K. Geim, S. V. Morozov, D. Jiang, Y. Zhang, S. V. Dubonos, I. V. Grigorieva, and A. A. Firsov, "Electric field effect in atomically thin carbon films.," *Science*, vol. 306, no. 5696, pp. 666–9, Oct. 2004.

[19]   K. S. Novoselov, A. K. Geim, S. V. Morozov, D. Jiang, M. I. Katsnelson, I. V Grigorieva, S. V. Dubonos, and A. A. Firsov, "Two-dimensional gas of massless Dirac fermions in graphene.," *Nature*, vol. 438, no. 7065, pp. 197–200, Nov. 2005.

[20]   A. Drabińska, A. Wołoś, M. Kamińska, W. Strupinski, and J. M. Baranowski, "Microwave studies of weak localization and antilocalization in epitaxial graphene," *AIP Conf. Proc.*, vol. 1566, pp. 159–160, 2013.

[21]   E. Karpierz, A. Drabińska, R. Bożek, P. Kaźmierczak, A. Wysmołek, M. Kamińska, and W. Strupiński, "ESR Spectroscopy of Graphene with Adsorbed NaCl Particles," *Acta Phys. Pol. A*, vol. 126, no. 5, pp. 1187–1189, Nov. 2014.

[22]   J. Kierdaszuk, P. Kaźmierczak, A. Drabińska, A. Wysmołek, K. Korona, M. Kamińska, K. Pakuła, I. Pasternak, A. Krajewska, and Z. R. Żytkiewicz, "Optical and Electrical Studies of Graphene Deposited on GaN Nanowires," *Acta Phys. Pol. A*, vol. 126, no. 5, pp. 1087–1089, Nov. 2014.

[23] B. Altshuler, D. Khmel'nitzkii, A. Larkin, and P. Lee, "Magnetoresistance and Hall effect in a disordered two-dimensional electron gas," *Phys. Rev. B*, vol. 22, no. 11, pp. 5142–5153, Dec. 1980.

[24] S. V. Morozov, K. S. Novoselov, M. I. Katsnelson, F. Schedin, L. A. Ponomarenko, D. Jiang, and A. K. Geim, "Strong Suppression of Weak Localization in Graphene," *Phys. Rev. Lett.*, vol. 97, no. 1, p. 016801, Jul. 2006.

[25] E. McCann, K. Kechedzhi, V. I. Fal'ko, H. Suzuura, T. Ando, and B. L. Altshuler, "Weak-Localization Magnetoresistance and Valley Symmetry in Graphene," *Phys. Rev. Lett.*, vol. 97, no. 14, p. 146805, Oct. 2006.

[26] J. M. B. Lopes dos Santos, N. M. R. Peres, and a. H. Castro Neto, "Graphene Bilayer with a Twist: Electronic Structure," *Phys. Rev. Lett.*, vol. 99, no. 25, p. 256802, Dec. 2007.

[27] S. Latil, V. Meunier, and L. Henrard, "Massless fermions in multilayer graphitic systems with misoriented layers: Ab initio calculations and experimental fingerprints," *Phys. Rev. B*, vol. 76, no. 20, p. 201402, Nov. 2007.

[28] C. Riedl and U. Starke, "Structural properties of the graphene-SiC(0001) interface as a key for the preparation of homogeneous large-terrace graphene surfaces," *Phys. Rev. B*, vol. 76, no. 24, p. 245406, Dec. 2007.

[29] K. V Emtsev, F. Speck, T. Seyller, and L. Ley, "Interaction , growth , and ordering of epitaxial graphene on SiC { 0001 } surfaces : A comparative photoelectron spectroscopy study," *Phys. Rev. B*, vol. 77, p. 155303, 2008.

[30] C. Riedl, C. Coletti, T. Iwasaki, A. A. Zakharov, and U. Starke, "Quasi-Free-Standing Epitaxial Graphene on SiC Obtained by Hydrogen Intercalation," *Phys. Rev. Lett.*, vol. 103, no. 24, p. 246804, Dec. 2009.

[31] K. Momma and F. Izumi, "VESTA 3 for three-dimensional visualization of crystal, volumetric and morphology data," *J. Appl. Crystallogr.*, vol. 44, no. 6, pp. 1272–1276, Oct. 2011.

[32] B. Jouault, B. Jabakhanji, N. Camara, W. Desrat, C. Consejo, and J. Camassel, "Interplay between interferences and electron-electron interactions in epitaxial graphene," *Phys. Rev. B*, vol. 83, no. 19, p. 195417, May 2011.

[33] S. Lara-Avila, A. Tzalenchuk, S. Kubatkin, R. Yakimova, T. J. B. M. Janssen, K. Cedergren, T. Bergsten, and V. I. Fal'ko, "Disordered Fermi Liquid in Epitaxial Graphene from Quantum Transport Measurements," *Phys. Rev. Lett.*, vol. 107, no. 16, p. 166602, Oct. 2011.

[34] E. McCann and V. I. Fal'ko, "z→-z Symmetry of Spin-Orbit Coupling and Weak Localization in Graphene," *Phys. Rev. Lett.*, vol. 108, no. 16, p. 166606, Apr. 2012.

[35] A. A. Kozikov, D. W. Horsell, E. McCann, and V. I. Fal'ko, "Evidence for spin memory in the electron phase coherence in graphene," *Phys. Rev. B*, vol. 86, no. 4, p. 045436, Jul. 2012.

[36] A. Drabińska, A. Babiński, T. Tomaszewicz, R. Bożek, and J. M. Baranowski, "Optical determination of the dopant concentration in the δ-doping layer," *J. Appl. Phys.*, vol. 92, no. 1, p. 163, 2002.

[37] A. Drabińska, K. P. Korona, R. Bożek, A. Babiński, J. M. Baranowski, W. Pacuski, R. Stępniewski, and T. Tomaszewicz, "Determination of Si ?-Doping Concentration in GaN by Electroreflectance," *Phys. status solidi*, vol. 234, no. 3, pp. 868–871, Dec. 2002.

[38] A. Drabińska, K. P. Korona, R. Bożek, J. M. Baranowski, K. Pakuła, T. Tomaszewicz, and J. Gronkowski, "Investigation of 2D Electron Gas on AlGaN/GaN Interface by Electroreflectance," *Phys. status solidi*, vol. 0, no. 1, pp. 329–333, 2003.

[39]   A. Drabińska, J. Borysiuk, W. Strupinski, and J. M. Baranowski, "Optical Transmission of Epitaxial Graphene Layers on SiC in the Visible Spectral Range," *Mater. Sci. Forum*, vol. 645–648, pp. 615–618, Apr. 2010.

[40]   A. Drabińska, K. Grodecki, W. Strupinski, R. Bożek, K. P. Korona, A. Wysmołek, R. Stępniewski, and J. M. Baranowski, "Growth kinetics of epitaxial graphene on SiC substrates," *Phys. Rev. B*, vol. 81, no. 24, p. 245410, Jun. 2010.

[41]   W. Strupinski, A. Drabińska, R. Bożek, J. Borysiuk, A. Wysmołek, R. Stępniewski, K. Kościewicz, P. Caban, K. P. Korona, K. Grodecki, P. A. Geslin, and J. M. Baranowski, "Growth Rate and Thickness Uniformity of Epitaxial Graphene," *Mater. Sci. Forum*, vol. 645–648, pp. 569–572, Apr. 2010.

[42]   K. Grodecki, A. Drabińska, R. Bożek, A. Wysmołek, and K. P. Korona, "Optical Absorption and Raman Scattering Studies of Few-Layer Epitaxial Graphene Grown on 4H-SiC Substrates," *Acta Phys. Pol. A*, vol. 116, no. 5, pp. 835–837, 2009.

[43]   K. Grodecki, J. Blaszczyk, W. Strupinski, A. Wysmołek, R. Stępniewski, A. Drabińska, M. Sochacki, A. Dominiak, and J. M. Baranowski, "Pinned and unpinned epitaxial graphene layers on SiC studied by Raman spectroscopy," *J. Appl. Phys.*, vol. 111, no. 11, p. 114307, 2012.

[44]   M. Tokarczyk, G. Kowalski, H. Kępa, K. Grodecki, A. Drabińska, and W. Strupinski, "Multilayer graphene stacks grown by different methods-thickness measurements by X-ray diffraction, Raman spectroscopy and optical transmission," *Crystallogr. Reports*, vol. 58, no. 7, pp. 1053–1057, Dec. 2013.

[45]   A. Wołoś, Z. Wilamowski, C. Skierbiszewski, A. Drabińska, B. Lucznik, I. Grzegory, and S. Porowski, "Electron spin resonance and Rashba field in GaN-based materials," *Phys. B Condens. Matter*, vol. 406, no. 13, pp. 2548–2554, Jul. 2011.

[46]   A. Wołoś, S. Szyszko, A. Drabińska, M. Kamińska, S. G. Strzelecka, A. Hruban, A. Materna, and M. Piersa, "Landau-Level Spectroscopy of Relativistic Fermions with Low Fermi Velocity in the $Bi_{2}Te_{3}$ Three-Dimensional Topological Insulator," *Phys. Rev. Lett.*, vol. 109, no. 24, p. 247604, Dec. 2012.

[47]   A. Wołoś, A. Drabińska, S. Szyszko, M. Kamińska, S. G. Strzelecka, A. Hruban, A. Materna, and M. Piersa, "Three-dimensional topological insulators Bi[sub 2]Te[sub 3], Bi[sub 2]Se[sub 3], and Bi[sub 2]Te[sub 2]Se - a microwave spectroscopy study," *AIP Conf. Proc.*, vol. 1566, pp. 197–198, 2013.